

Enhanced Photovoltaic Performances of Graphene/Si Solar Cells by Insertion of an MoS₂ Thin Film

Yuka Tsuboi[†], Feijiu Wang[†], Daichi Kozawa[†], Kazuma Funahashi[‡],

Shinichiro Mouri[†], Yuhei Miyauchi^{†§}, Taishi Takenobu[‡] and Kazunari Matsuda^{†}*

[†]Institute of Advanced Energy, Kyoto University, Gokasho, Uji, Kyoto 611-0011, Japan

[‡]Department of Advanced Science and Engineering, Waseda University, Shinjuku-ku, Tokyo
169-8555, Japan

[§]JST, ERATO, Itami Molecular Nanocarbon Project, Nagoya University, Chikusa, Nagoya 464-
8602, Japan

ABSTRACT

Atomically thin layered materials such as graphene and transition-metal dichalcogenides exhibit great potential as active materials in optoelectronic devices because of their high carrier-transporting properties and strong light–matter interactions. Here, we demonstrated that the

photovoltaic performances of graphene/Si Schottky junction solar cells were significantly improved by inserting a chemical vapor deposition (CVD)-grown, large MoS₂ thin-film layer. This layer functions as an effective passivation and electron-blocking/hole-transporting layer. We also demonstrated that the photovoltaic properties are enhanced with increasing number of graphene layers and decreasing thickness of the MoS₂ layer. A high photovoltaic conversion efficiency of 11.1% was achieved with the optimized trilayer-graphene/MoS₂/n-Si solar cell.

Keywords: solar cell, molybdenum disulfide (MoS₂), two-dimensional material, graphene, Schottky junction

TEXT

With an increase in low dimensional material research, these atomically thin materials have been widely and intensively studied from the viewpoints of both fundamental physics and applications.¹⁻⁸ Transition-metal dichalcogenides (TMDs) (MX_2 ; $M = \text{Mo, W}$; $X = \text{Se, S}$) are among the most attractive two-dimensional (2D) layered materials that can be thinned down to atomic-scale thickness.⁹ Monolayer molybdenum disulfide (MoS₂), which is a typical and well-studied TMD system, is a direct bandgap semiconductor, whereas bulk MoS₂ is an indirect bandgap semiconductor. The direct-to-indirect energy-gap transition occurs in MoS₂ when it changes from a monolayer to a bilayer, and the optical bandgap changes from 1.8 eV in monolayer MoS₂ to 1.2 eV in bulk MoS₂.^{3,10,11} The optical band gap associated with their energy

structures in MoS₂ can be changed by manipulation of the layer numbers, which has potential applications of various optical and electronic devices.¹²⁻¹⁴

2D materials are used as building blocks to fabricate artificial multi-junction nanostructures because layered 2D materials with an atomically flat surface can be easily stacked by van der Waals interactions. Artificial multi-junction nanostructures composed of various 2D materials with novel characteristics can be fabricated. Indeed, graphene on *h*-BN exhibits an extremely high carrier mobility that exceeds 60,000 cm²V⁻¹s⁻¹,¹⁵ which is much larger than that of graphene on an SiO₂/Si substrate. Very high photo-responsivity has also been reported for optoelectronic devices based on the stacking of graphene and MoS₂ (graphene/MoS₂).¹⁶⁻¹⁸ The graphene/MoS₂ heterostructure is considered a promising platform for photovoltaic applications.¹⁹⁻²² The photovoltaic properties of solar cells based on low dimensional carbon materials and Si heterojunctions have been intensively studied.²³⁻²⁶ In the case of graphene/Si solar cell, the approaches used to improve photovoltaic performance have primarily involved carrier doping in the graphene layer, the insertion of an oxide layer, or the deposition of an antireflection layer onto the surface of a solar cell.²⁷⁻³³

In this study, we investigate the photovoltaic properties of graphene/MoS₂/*n*-Si solar cells. The photovoltaic properties were considerably enhanced by the insertion of chemical vapor deposition (CVD)-grown large MoS₂ thin film, which functions as an effective passivation and electron-blocking/hole-transporting layer. The optimized graphene/MoS₂/*n*-Si solar cell exhibited a high photovoltaic conversion efficiency of 11.1%, which is a remarkable conversion efficiency in a photovoltaic device using MoS₂ thin film.

RESULTS AND DISCUSSION

Figure 1(a) shows a schematic of the graphene/MoS₂/*n*-Si solar cell. It comprises the two types of 2D materials, CVD-grown MoS₂ film and graphene, stacked on a patterned *n*-type SiO₂/Si substrate (with a $\phi = 1$ mm window). Large-scale MoS₂ films for solar cells were fabricated by the CVD method.³⁴⁻³⁶ As a first step, an MoO₃ (99.98%, Sigma-Aldrich) film with the desired thickness was fabricated on an SiO₂/Si substrate using the thermal-evaporation technique under vacuum conditions ($\sim 10^{-3}$ Pa); this MoO₃ film was subsequently sulfurized. The sulfurization step of the MoO₃ film was conducted using the CVD furnace. The SiO₂/Si substrate with an MoO₃ film was placed in the center of a quartz tube, and sulfur (>98%, Wako) was loaded at the upstream side. The substrate was heated by the CVD furnace to 750 °C at a heating rate of 15 °C/min and maintained at this temperature for 30 min. At the growth temperature (750 °C), sulfur was also heated to 190 °C using a ribbon heater, resulting in sulfur transport. All processes were performed under high-purity Ar gas flow flowing at 50 sccm under ambient conditions. We fabricated MoS₂ films with various thicknesses on SiO₂/Si substrates, as shown in Figure S1.

The graphene/MoS₂/*n*-Si solar cells were fabricated by transferring CVD-grown MoS₂ films and graphene films (single-layer graphene, Graphene Platform) onto the *n*-type Si substrate (1–5 $\Omega \cdot \text{cm}^{-1}$) with an ~ 300 -nm-thick SiO₂ layer. A circular window with a diameter of 1 mm was patterned on the SiO₂/Si substrate. This Si substrate was dipped into buffered hydrofluoric acid (HF) solutions for several seconds to remove the natural oxidation layer on the window, which obstructs the electrical contact. The MoS₂ film was then transferred *via* thermal release tape (REVALPHA; No. 3195MS, Nitto Denko). In this study, the transfer process using the thermal release tape was a more facile method compared with the conventional method of using a

polymer support film.^{37,38} In Figure S2, we show the MoS₂ transfer process in detail. For the fine transfer, the first key step is peeling the CVD-grown MoS₂ film from the growth substrate. The water droplet facilitates clear peeling because of the difference in hydrophobicities between the SiO₂/Si substrate and the MoS₂ film.³⁹ In this transfer method, the process is completed quickly, because the MoS₂ film can be released from the tape by heating, thereby eliminating the need to expose the film to a solution for a prolonged period.

Subsequently, we transferred graphene layers onto MoS₂/*n*-Si. Poly(bisphenol A carbonate) dissolved in chloroform (3 wt%) was spin-coated onto the single-layer graphene deposited onto copper foil for the transfer process. The graphene film was floated on FeCl₃ to etch out the copper foil and was subsequently transferred to the MoS₂/*n*-Si substrate.³⁷ The graphene/MoS₂/*n*-Si was baked at 120 °C for 5 min, and the polymer layer was then dissolved in chloroform. Finally, Au was deposited as an electrode onto the surface of the graphene/MoS₂/*n*-Si, with the exception of the window region, *via* the Ar-ion sputtering method. Indium (In), as the cathode, was soldered onto the back side of the solar cell. The process of fabricating the graphene/MoS₂/*n*-Si solar cell is described in the Supporting Information.

Figure 2(a) shows the Raman spectrum of the CVD-grown MoS₂ film. The spectrum shows several Raman peaks, including the in-plane E_{2g}¹ mode (~383 cm⁻¹) and the out-of-plane A_{1g} (~408 cm⁻¹) mode of MoS₂. The frequency difference between the E_{2g}¹ and A_{1g} Raman peaks (~25 cm⁻¹) are consistent with the previously reported values for bulk MoS₂,^{40,41} which suggests that the MoS₂ film used in this study is relatively thick, as described below in detail. The Raman spectrum of the graphene/MoS₂ structures also indicates the vertical stacking of graphene/MoS₂ (see Supporting Figure S3).

Figure 2(b) shows the absorption spectrum of the MoS₂ film deposited on the quartz substrate. Distinct absorption peaks around 680 nm and 640 nm are observed in the spectrum, which are assigned as A exciton (680 nm) and B exciton (640 nm) peaks associated with the direct bandgap transitions at the K point of MoS₂ in the momentum space. Also, we observed the intense C peak at ~460 nm. This peak arises from the distinguishing band structure (band nesting), which is the parallel region of the conduction and valence bands.^{20,42,43}

Figure 2(c) shows the surface morphology of MoS₂ films measured by atomic force microscopy (AFM). The surface of CVD-grown MoS₂ films shows the assembly of small grains with a typical lateral size of ~30 nm and a roughness of ~6.5 nm. We also investigated the thickness of the MoS₂ films using AFM. Figure S1(c) shows AFM images measured at the step edge of a typical MoS₂ film used for devices and deposited onto a Si substrate. The inset of Figure 2(d) shows the profile at the line in the figure. The thickness of this MoS₂ film was evaluated as ~17 nm on the basis of this height profile, which corresponds to a film with ~20 MoS₂ layers because the thickness of a monolayer of MoS₂ is ~0.7 nm.^{40,44} The evaluated thickness is consistent with the Raman spectral data (Figure 2(a)) and with the absorption spectra (Figure 2(b)). In particular, we fabricated MoS₂ films with various thicknesses as shown in Figure S1(b) and (c).

We conducted X-ray photoelectron spectroscopy (XPS) of fabricated MoS₂ films to verify the absence of residual ingredients. The XPS spectrum in Figure 2(d) shows several peaks of the Mo 3d and S 2s core levels. The Mo 3d XPS spectrum is also shown in the inset of Figure 2(d), which indicates that the peaks at 162.6, 229.8, and 232.8 eV are associated with the S 2s, Mo 3d_{5/2}, and Mo 3d_{3/2} core levels. The binding energies of these peaks are consistent with the previously reported values of Mo⁴⁺ and S²⁻ in MoS₂.^{45,46} The Raman, optical absorption, AFM,

and XPS data, as shown in Figure 2(a)–(d), certify that MoS₂ films were definitely deposited *via* the CVD method.

Figure 3(a) shows the current-density–voltage (J – V) curves of the monolayer-graphene/MoS₂/ n -Si solar cell under dark and AM 1.5 illumination conditions. The J – V curve of the monolayer-graphene/MoS₂/ n -Si solar cell under the dark condition (gray line) exhibits typical diode behavior. Furthermore, the monolayer-graphene/MoS₂/ n -Si solar cell (yellow line) exhibits clear photovoltaic properties. The open-circuit voltage V_{OC} , short-circuit current density J_{SC} , and fill factor FF of the cell are 0.41 V, 13.1 mA·cm⁻², 0.25, respectively, which results in a photovoltaic conversion efficiency (η) of 1.35%. The inset of Figure 3(a) shows the J – V curves of a graphene/ n -Si solar cell without an MoS₂ layer, where the fabrication process and materials were same as those used to fabricate the monolayer-graphene/MoS₂/ n -Si cell. The photovoltaic parameters, V_{OC} , J_{SC} , and FF are 0.22 V, 1.9 mA·cm⁻², and 0.18, respectively, which result in a photovoltaic conversion efficiency (η) of 0.07%. All the photovoltaic parameters of the graphene/MoS₂/ n -Si solar cell are increased in comparison to those of the graphene/ n -Si solar cell in our experiments, which suggests that the MoS₂ layer plays an important role in enhancing the photovoltaic performance of solar cells.

We varied the layer thicknesses of MoS₂ in the graphene/MoS₂/ n -Si solar cells. Figure 3 shows the J – V curves of graphene/MoS₂/ n -Si solar cells with different numbers of graphene layers when illuminated under the AM 1.5 condition. The red, orange, and yellow lines in Figure 3(b) corresponds to J – V curve of graphene/MoS₂/ n -Si solar cells with monolayer, bilayer, and trilayer graphene, respectively, where we controlled the number of graphene layers by changing the number of times the graphene transfer process was conducted. The photovoltaic properties of

graphene/MoS₂/*n*-Si solar cells increased with increasing number of graphene layers. The trilayer-graphene/MoS₂/*n*-Si solar cells exhibit a V_{OC} , J_{SC} , and FF of 0.54 V, 28.1 mA·cm⁻², and 0.53, which results in a high photovoltaic efficiency of 8.0%.

These parameters of monolayer- and bilayer-graphene/MoS₂/*n*-Si solar cells and the series resistance estimated from the slope of each $J-V$ curve are shown in Table 1 of Supporting Information S4. The series resistance of the solar cells drastically decreased with increasing number of graphene layers, consistent with the previously reported results of decreased sheet resistance in graphene layers.⁴⁷ Our results suggest that the decrease in series resistance is responsible for the reduction of loss, which contributes to the enhancement of photovoltaic conversion efficiency in graphene/MoS₂/*n*-Si solar cells.

The incident photon to current conversion efficiency (IPCE) spectra revealed that MoS₂ functions as a shading layer at the point of light absorption, as shown in Supporting Information S5. Thus, the generated carriers in the *n*-Si layer are the main contributors to the photovoltaic current in the cell. Therefore, the enhancement of photovoltaic performance by the insertion of an MoS₂ layer implies that the MoS₂ layer serves positive roles as both an effective passivation layer and a hole-transporting/electron-blocking layer in the photovoltaic process, as described below in detail.

The MoS₂ plays an important role of passivation layer for separation the graphene and Si to reduce the interface carrier recombination. The tunneling barrier effect by the passivation layer with a thickness of several nanometers to several tenths of nanometers prevents direct contact between the semiconductor and conductive layers and can thereby suppress the recombination losses at the interface. The tunneling barrier thickness also plays a key role in determining device

performance.⁴⁸ We fabricated a trilayer-graphene/MoS₂/*n*-Si solar cell using a thinner (~9 nm) MoS₂ film. Figure 4 shows the J - V curve for the graphene/MoS₂/*n*-Si solar cell. The optimized graphene/MoS₂/*n*-Si solar cells exhibit V_{OC} , J_{SC} , and FF photovoltaic parameters of 0.56 V, 33.4 mA·cm⁻², and 0.60, which results in a high photovoltaic efficiency of 11.1%. This value of 11.1% is among the highest efficiencies reported for a solar cell containing an MoS₂ layer. Thinner layer is suitable not only for passivation effect but also for shadow effect by MoS₂ layer. This improvement indicates that more photons passed through the MoS₂ and were absorbed by the Si.

To better understand the photovoltaic process, we constructed band alignment diagrams for the graphene/*n*-Si and graphene/MoS₂/*n*-Si solar cells, as shown in Figure 5. Figure 5(a) shows the band alignment of a graphene/*n*-Si solar cell under ambient conditions, where the graphene has been *p*-doped *via* the FeCl₃ etching process.⁴⁹⁻⁵¹ The photovoltaic process in the graphene/*n*-Si solar cells is understood by the Schottky barrier formed at the semimetal (graphene) and semiconductor (*n*-Si) interface. Figure 5(b) shows a schematic band diagram for graphene/MoS₂/*n*-Si solar cells. We confirmed that the CVD-grown MoS₂ exhibits *n*-type properties on the basis of the transfer characteristics of the electric double-layer transistor (Supporting Information S6).⁵² The insertion of an MoS₂ layer into graphene/*n*-Si solar cells modifies the band alignment. Indeed, the photovoltaic properties are enhanced by the insertion of an MoS₂ layer, as shown in Figure 3(a). The total built-in voltage (V_{bi}) of graphene/MoS₂/*n*-Si solar cells is greater than that of the graphene/*n*-Si solar cell because the Schottky barrier height is determined by the energy difference between the electron affinity χ_s of the semiconductor and the work function W_m of graphene, *i.e.*, $W_m - \chi_s$.⁵³⁻⁵⁵ The increase of the built-in field by insertion of an MoS₂ layer can directly improve the V_{OC} and the photovoltaic conversion

efficiency. Moreover, because of the difference between Fermi levels, the bottom of the conduction band and the top of the valence band of the MoS₂ layer at the interface of graphene are shifted upward, resulting in the energy barrier at the interface between MoS₂ and *n*-Si. The energy barrier of the MoS₂ layer functions as an effective electron blocking layer for the photogenerated electrons in the Si layer. Furthermore, in the case of the photogenerated hole, the energy barrier created by the MoS₂ layer functions as an effective hole-transport layer. The effective carrier transporting (blocking) layer of MoS₂ effectively reduces the recombination loss of carriers, which in turn results in an increase of the J_{SC} . Therefore, the MoS₂ layer between the graphene and *n*-Si contribute to the enhancement of photovoltaic performance as a carrier transporting (blocking) layer, as shown in Figure 3(a).

CONCLUSIONS

In summary, we investigated the considerable enhancement of the photovoltaic performance of graphene/Si solar cells using the 2D material MoS₂. The large-area CVD-grown MoS₂ films enabled the fabrication of graphene/MoS₂/*n*-Si solar cells. The MoS₂ acts as both an effective passivation layer and hole-transporting/electron-blocking layer, which contributes to the remarkable conversion efficiency of 11.1% in the fabricated graphene/MoS₂/*n*-Si solar cells. This result opens new directions for MoS₂ research and the potential use of MoS₂ in various optoelectronic applications.

MATERIALS AND METHODS

Raman spectrum of the MoS₂ films was obtained using a laser Raman microscope (Nanophoton, RAMANtouch). The optical absorption spectrum of the MoS₂ films on the glass substrates was measured using a UV/Vis spectrophotometer (SHIMADZU, UV-1800). XPS was conducted on a TRXPS spectrometer (JEOL, JPS-9010TRX). The surface morphologies were measured by AFM (Agilent Technologies). To test the photovoltaic performance, the solar cells were irradiated using a solar simulator (San-Ei Electric XES-40S1) under AM 1.5 conditions (100 mW·cm⁻²) and the current density–voltage data were recorded using a source meter (Keithley 2400). The AM 1.5 condition for the solar simulator was confirmed using a standard cell (BS-500BK). For the incident-to-photon conversion efficiency (IPCE) measurements, the devices were tested using a monochromated xenon arc light system (Zolix LSP-X150).

Conflict of Interest: The authors declare no competing financial interest.

FIGURES

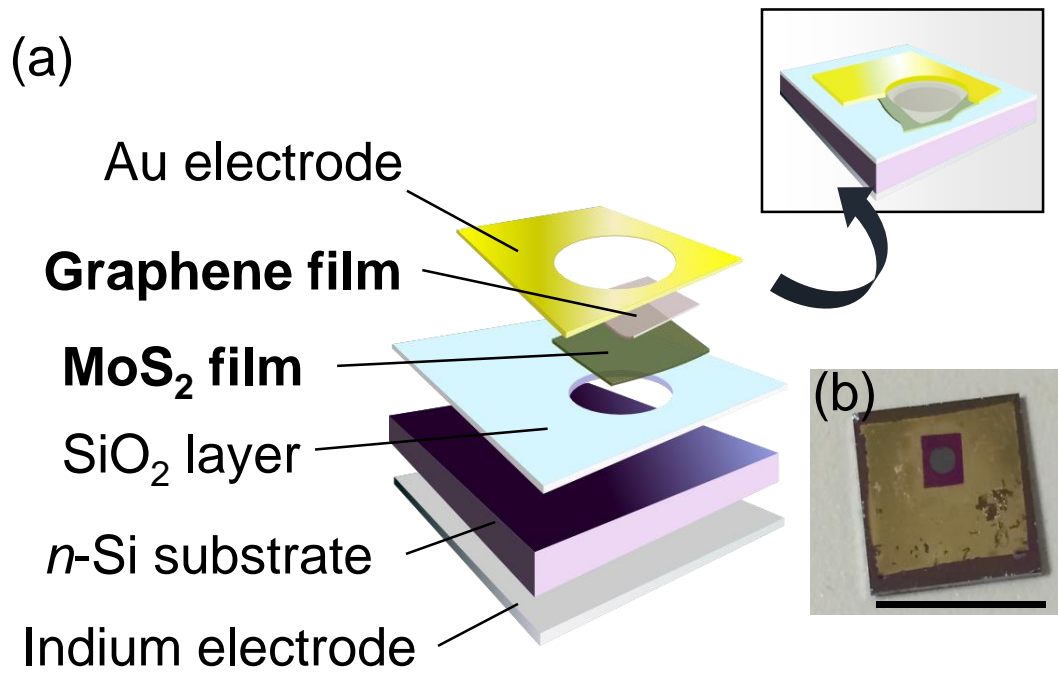


Fig. 1 Y. Tsuboi *et al.*

Figure 1. (a) Schematic of the graphene/MoS₂/n-Si solar cell. (b) An optical image of a graphene/MoS₂ thin film deposited onto a substrate. The scale bar is 1 cm.

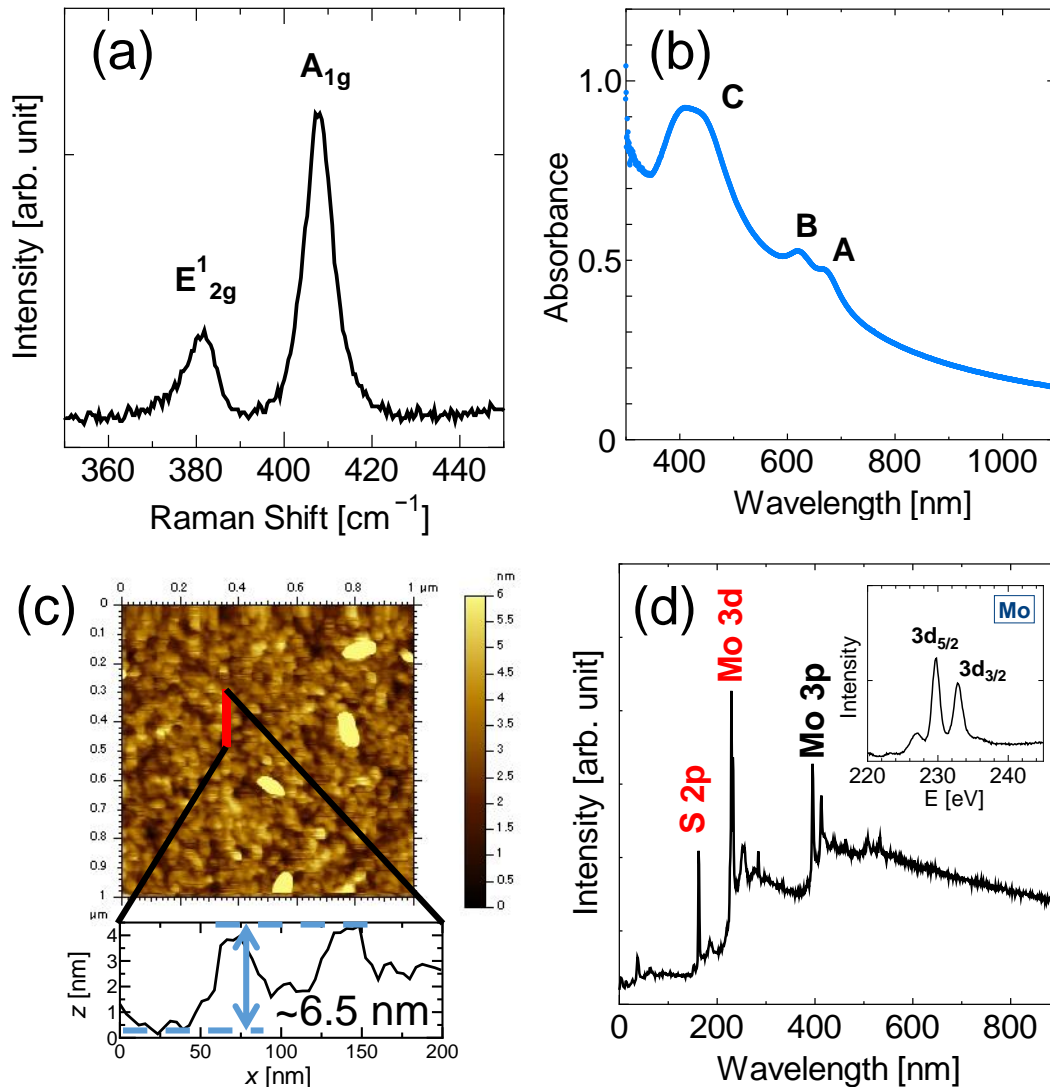


Fig. 2 Y. Tsuboi *et al.*

Figure 2. Characterization of CVD-grown MoS₂ film. (a) Raman spectra of MoS₂ films. The two Raman peaks associated with MoS₂, an in-plane (E_{12g}) mode at 383 cm⁻¹ and an out-of-plane (A_{1g}) mode at 408 cm⁻¹, are observed. (b) Optical absorption spectra of MoS₂. Distinct absorption peaks associated with A and B excitons are observed. (c) AFM image of an as-grown MoS₂ film. The height profile in the line is shown in the Figure. (d) X-ray photoelectron spectrum of an MoS₂ film showing Mo and S peaks. The inset is the Mo 3d spectrum.

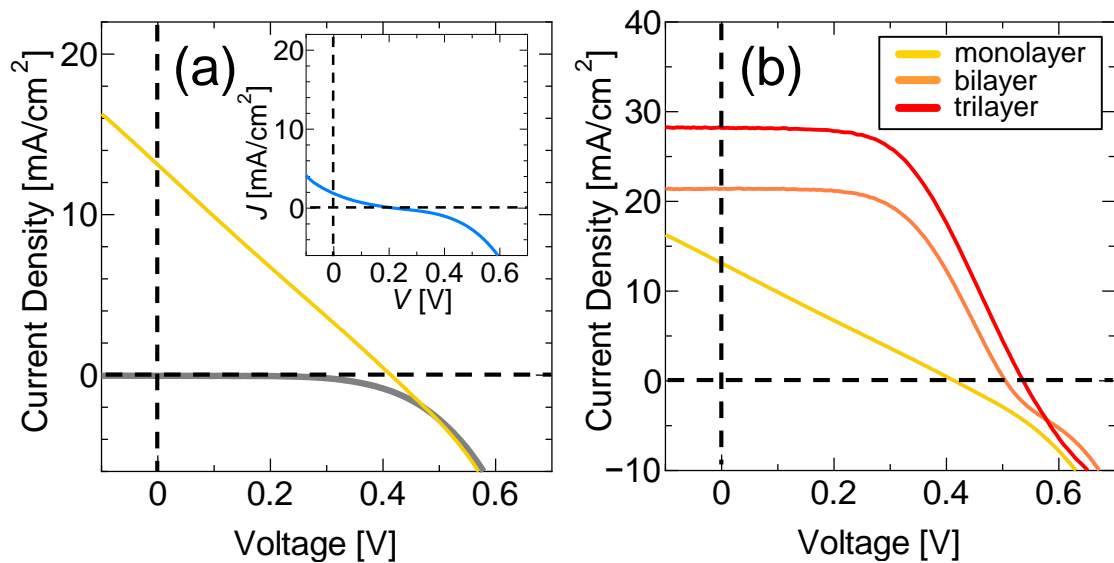


Fig. 3 Y. Tsuboi *et al.*

Figure 3. Photovoltaic performance of monolayer-, bilayer-, and trilayer-graphene/MoS₂/n-Si solar cells. (a) Current density–voltage (J - V) curves of a monolayer-graphene/MoS₂/n-Si solar cell under darkness (gray line) and under AM 1.5 illumination conditions (yellow line). The J - V curve of a bilayer-graphene/n-Si solar cell under AM 1.5 illumination is also shown in the inset. (b) J - V curves of monolayer-, bilayer-, and trilayer-graphene/MoS₂/n-Si solar cells, where the number of graphene layers was controlled by the number of graphene transfer processes performed.

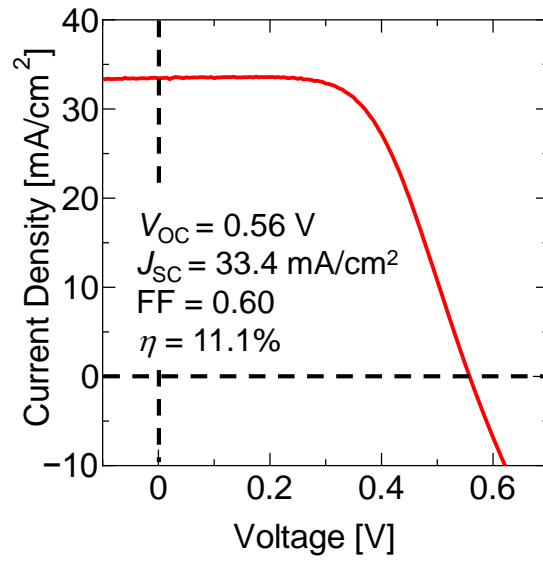


Fig. 4 Y. Tsuboi *et al.*

Figure 4. The current density–voltage (J – V) curves of a trilayer-graphene/MoS₂/ n -Si solar cell with a 9-nm-thick MoS₂ layer; the curves were measured under AM 1.5 illumination conditions. Photovoltaic parameters, including the open-circuit voltage V_{OC} , short-circuit current density J_{SC} , fill factor FF, and photovoltaic efficiency η determined from this curve are indicated in the Figure.

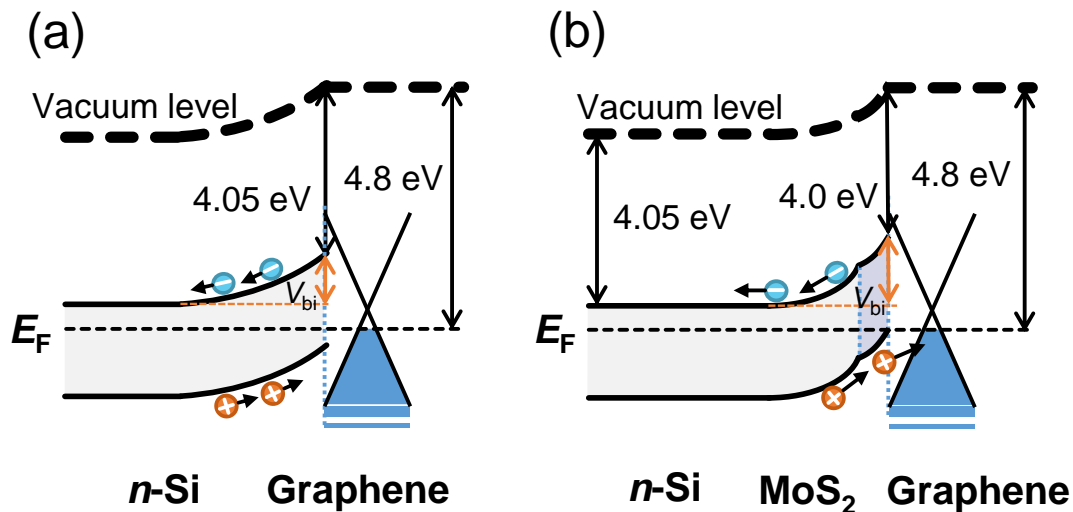


Fig. 5 Y. Tsuboi *et al.*

Figure 5. Schematics of band diagrams for the solar cells. The photovoltaic processes (a) in the graphene/ n -Si and (b) in the graphene/MoS₂/ n -Si solar cells are shown.

AUTHOR INFORMATION

Corresponding Author

matsuda@iae.kyoto-u.ac.jp

ACKNOWLEDGMENT

Part of this work was supported by M. Endo, A. Wakamiya, Y. Murata, T. Nakata, and T. Morii for experimental equipment. We also thank to Nitto Denko Corporation for providing us thermal release tape. This study was supported by a Grant-in-Aid for Scientific Research from the Japan Society for Promotion of Science (Grants Nos. 24681031, 22740195, 22016007, 25000003, and

23340085), the Precursory Research for Embryonic Science and Technology program from the Japan Science and Technology Agency, the Yazaki Memorial Foundation for Science and Technology, the Nippon Sheet Glass Foundation for Materials Science and Engineering, and The Canon Foundation. KF acknowledges the Leading Graduate Program in Science and Engineering, Waseda University from MEXT, Japan.

Supporting Information Available: Characterization of MoS₂ film, process-flow of MoS₂ film transfer, photovoltaic parameters of graphene/MoS₂/n-Si solar cells, and carrier transport properties of MoS₂ films.

REFERENCES

1. Geim, A. K.; Novoselov, K. S., The Rise of Graphene. *Nat. Mater.* **2007**, *6*, 183-191.
2. Splendiani, A.; Sun, L.; Zhang, Y.; Li, T.; Kim, J.; Chim, C.-Y.; Galli, G.; Wang, F., Emerging Photoluminescence in Monolayer MoS₂. *Nano Lett.* **2010**, *10*, 1271-1275.
3. Radisavljevic, B.; Radenovic, A.; Brivio, J.; Giacometti, V.; Kis, A., Single-layer MoS₂ Transistors. *Nat. Nanotechnol.* **2011**, *6*, 147-150.
4. Rao, C. N. R.; Sood, A. K.; Subrahmanyam, K. S.; Govindaraj, A., Graphen, Das Neue Zweidimensionale Nanomaterial. *Angew. Chem.* **2009**, *121*, 7890-7916.

5. He, Z.; Sheng, Y.; Rong, Y.; Lee, G.-D.; Li, J.; Warner, J. H., Layer-Dependent Modulation of Tungsten Disulfide Photoluminescence by Lateral Electric Fields. *ACS nano* **2015**, in press.
6. Saito, Y.; Iwasa, Y., Ambipolar Insulator-to-Metal Transition in Black Phosphorus by Ionic-Liquid Gating. *ACS nano* **2015**, in press.
7. Li, S.; Luo, Y.; Lv, W.; Yu, W.; Wu, S.; Hou, P.; Yang, Q.; Meng, Q.; Liu, C.; Cheng, H. M., Vertically Aligned Carbon Nanotubes Grown on Graphene Paper as Electrodes in Lithium-Ion Batteries and Dye-Sensitized Solar Cells. *Adv. Energy Mater.* **2011**, 1, 486-490.
8. Sun, D.-m.; Timmermans, M. Y.; Tian, Y.; Nasibulin, A. G.; Kauppinen, E. I.; Kishimoto, S.; Mizutani, T.; Ohno, Y., Flexible High-Performance Carbon Nanotube Integrated Circuits. *Nat. Nanotech.* **2011**, 6, 156-161.
9. Wilson, J. A.; Yoffe, A. D., The Transition Metal Dichalcogenides Discussion and Interpretation of the Observed Optical, Electrical and Structural Properties. *Adv. Phys.* **1969**, 18, 193-335.
10. Mak, K. F.; Lee, C.; Hone, J.; Shan, J.; Heinz, T. F., Atomically Thin MoS₂: A New Direct-Gap Semiconductor. *Phys. Rev. Lett.* **2010**, 105, 136805.
11. Chu, L.; Schmidt, H.; Pu, J.; Wang, S.; Özyilmaz, B.; Takenobu, T.; Eda, G., Charge Transport in Ion-Gated Mono-, Bi-, and Trilayer MoS₂ Field Effect Transistors. *Sci. Rep.* **2014**, 4, 7293

12. Beal, A. R.; Knights, J. C.; Liang, W. Y., Transmission Spectra of Some Transition Metal Dichalcogenides. II. Group VIA: Trigonal Prismatic Coordination. *J. Phys. C: Solid State Phys.* **1972**, 5, 3540.
13. Tsai, M.-L.; Su, S.-H.; Chang, J.-K.; Tsai, D.-S.; Chen, C.-H.; Wu, C.-I.; Li, L.-J.; Chen, L.-J.; He, J.-H., Monolayer MoS₂ Heterojunction Solar Cells. *ACS Nano* **2014**, 8, 8317-8322.
14. Shanmugam, M.; Durcan, C. A.; Yu, B., Layered Semiconductor Molybdenum Disulfide Nanomembrane Based Schottky-Barrier Solar Cells. *Nanoscale* **2012**, 4, 7399-7405.
15. Dean, C. R.; Young, A. F.; Meric, I.; Lee, C.; Wang, L.; Sorgenfrei, S.; Watanabe, K.; Taniguchi, T.; Kim, P.; Shepard, K. L., Boron Nitride Substrates for High-Quality Graphene Electronics. *Nat. Nanotechnol.* **2010**, 5, 722-726.
16. Yoon, Y.; Ganapathi, K.; Salahuddin, S., How Good Can Monolayer MoS₂ Transistors Be? *Nano Lett.* **2011**, 11, 3768-3773.
17. Wang, H.; Yu, L.; Lee, Y.-H.; Shi, Y.; Hsu, A.; Chin, M. L.; Li, L.-J.; Dubey, M.; Kong, J.; Palacios, T., Integrated Circuits Based on Bilayer MoS₂ Transistors. *Nano Lett.* **2012**, 12, 4674-4680.
18. Yin, Z.; Li, H.; Li, H.; Jiang, L.; Shi, Y.; Sun, Y.; Lu, G.; Zhang, Q.; Chen, X.; Zhang, H., Single-Layer MoS₂ Phototransistors. *ACS nano* **2011**, 6, 74-80.
19. Roy, K.; Padmanabhan, M.; Goswami, S.; Sai, T. P.; Ramalingam, G.; Raghavan, S.; Ghosh, A., Graphene-MoS₂ Hybrid Structures for Multifunctional Photoresponsive Memory Devices. *Nat. Nanotechnol.* **2013**, 8, 826-830.

20. Zhang, W.; Chuu, C.-P.; Huang, J.-K.; Chen, C.-H.; Tsai, M.-L.; Chang, Y.-H.; Liang, C.-T.; Chen, Y.-Z.; Chueh, Y.-L.; He, J.-H., Ultrahigh-Gain Photodetectors Based on Atomically Thin Graphene-MoS₂ Heterostructures. *Sci. Rep.* **2014**, *4*, 3826.
21. Roy, K.; Padmanabhan, M.; Goswami, S.; Sai, T. P.; Kaushal, S.; Ghosh, A., Optically Active Heterostructures of Graphene and Ultrathin MoS₂. *Solid State Commun.* **2013**, *175*, 35-42.
22. Chen, C.-C.; Aykol, M.; Chang, C.-C.; Levi, A. F. J.; Cronin, S. B., Graphene-Silicon Schottky Diodes. *Nano Lett.* **2011**, *11*, 1863-1867.
23. Li, X.; Zhu, H.; Wang, K.; Cao, A.; Wei, J.; Li, C.; Jia, Y.; Li, Z.; Li, X.; Wu, D., Graphene-on-Silicon Schottky Junction Solar Cells. *Adv. Mater.* **2010**, *22*, 2743-2748.
24. Xie, C.; Lv, P.; Nie, B.; Jie, J.; Zhang, X.; Wang, Z.; Jiang, P.; Hu, Z.; Luo, L.; Zhu, Z., Monolayer Graphene Film/Silicon Nanowire Array Schottky Junction Solar Cells. *Appl. Phys. Lett.* **2011**, *99*, 133113.
25. Cui, K.; Anisimov, A. S.; Chiba, T.; Fujii, S.; Kataura, H.; Nasibulin, A. G.; Chiashi, S.; Kauppinen, E. I.; Maruyama, S., Air-Stable High-Efficiency Solar Cells with Dry-Transferred Single-Walled Carbon Nanotube Films. *J. Mater. Chem. A* **2014**, *2*, 11311-11318
26. F. Wang, D. Kozawa, Y. Miyauchi, K. Hiraoka, S. Mouri, Y. Ohno, K. Matsuda *ACS Photonics* **2014**, *1*, 360-364.
27. Miao, X.; Tongay, S.; Petterson, M. K.; Berke, K.; Rinzler, A. G.; Appleton, B. R.; Hebard, A. F., High Efficiency Graphene Solar Cells by Chemical Doping. *Nano Lett.* **2012**, *12*, 2745-2750.

28. Li, X.; Xie, D.; Park, H.; Zhu, M.; Zeng, T. H.; Wang, K.; Wei, D.; Kong, J.; Zhu, H., Ion Doping of Graphene for High-Efficiency Heterojunction Solar Cells. *Nanoscale* **2013**, 5, 1945-1948.
29. Cui, T.; Lv, R.; Huang, Z.-H.; Chen, S.; Zhang, Z.; Gan, X.; Jia, Y.; Li, X.; Wang, K.; Wu, D., Enhanced Efficiency of Graphene/Silicon Heterojunction Solar Cells by Molecular Doping. *J. Mater. Chem. A* **2013**, 1, 5736-5740.
30. Yang, L.; Yu, X.; Xu, M.; Chen, H.; Yang, D., Interface Engineering for Efficient and Stable Chemical-Doping-Free Graphene-on-Silicon Solar Cells by Introducing a Graphene Oxide Interlayer. *J. Mater. Chem. A* **2014**, 2, 16877-16883.
31. Shi, E.; Li, H.; Yang, L.; Zhang, L.; Li, Z.; Li, P.; Shang, Y.; Wu, S.; Li, X.; Wei, J., Colloidal Antireflection Coating Improves Graphene–Silicon Solar Cells. *Nano Lett.* **2013**, 13, 1776-1781.
32. Liu, X.; Zhang, X. W.; Yin, Z. G.; Meng, J. H.; Gao, H. L.; Zhang, L. Q.; Zhao, Y. J.; Wang, H. L., Enhanced Efficiency of Graphene-Silicon Schottky Junction Solar Cells by Doping with Au Nanoparticles. *Appl. Phys. Lett.* **2014**, 105, 183901.
33. Song, Y.; Li, X.; Mackin, C.; Zhang, X.; Fang, W.; Palacios, T.; Zhu, H.; Kong, J., Role of Interfacial Oxide in High-Efficiency Graphene-Silicon Schottky Barrier Solar Cells. *Nano Lett.* **2015**, in press.
34. Feijiu, W.; Daichi, K.; Yuhei, M.; Kazushi, H.; Shinichiro, M.; Yutaka, O.; Kazunari, M., Considerably Improved Photovoltaic Performance of Carbon Nanotube-Based Solar Cells Using Metal Oxide Layers. *Nat. Commun.* **2015**, 6, 6305.

35. Zhan, Y.; Liu, Z.; Najmaei, S.; Ajayan, P. M.; Lou, J., Large-Area Vapor-Phase Growth and Characterization of MoS₂ Atomic Layers on a SiO₂ Substrate. *Small* **2012**, 8, 966-971
36. Lee, Y. H.; Zhang, X. Q.; Zhang, W.; Chang, M. T.; Lin, C. T.; Chang, K. D.; Yu, Y. C.; Wang, J. T. W.; Chang, C. S.; Li, L. J., Synthesis of Large - Area MoS₂ Atomic Layers with Chemical Vapor Deposition. *Adv. Mater.* **2012**, 24, 2320-2325.
37. Wu, J.; Schmidt, H.; Amara, K. K.; Xu, X.; Eda, G.; Özyilmaz, B., Large Thermoelectricity *via* Variable Range Hopping in Chemical Vapor Deposition Grown Single-Layer MoS₂. *Nano Lett.* **2014**, 14, 2730-2734.
38. Reina, A.; Son, H.; Jiao, L.; Fan, B.; Dresselhaus, M. S.; Liu, Z.; Kong, J., Transferring and Identification of Single- and Few-Layer Graphene on Arbitrary Substrates. *J. Phys. Chem. C* **2008**, 112, 17741-17744.
39. Li, H.; Wu, J.; Huang, X.; Yin, Z.; Liu, J.; Zhang, H., A Universal, Rapid Method for Clean Transfer of Nanostructures onto Various Substrates. *ACS Nano* **2014**, 8, 6563-6570.
40. Li, H.; Zhang, Q.; Yap, C. C. R.; Tay, B. K.; Edwin, T. H. T.; Olivier, A.; Baillargeat, D., From Bulk to Monolayer MoS₂: Evolution of Raman Scattering. *Adv. Funct. Mater.* **2012**, 22, 1385-1390.
41. Lee, C.; Yan, H.; Brus, L. E.; Heinz, T. F.; Hone, J.; Ryu, S., Anomalous Lattice Vibrations of Single- and Few-Layer MoS₂. *ACS Nano* **2010**, 4, 2695-2700.

42. Kozawa, D.; Kumar, R.; Carvalho, A.; Amara, K. K.; Zhao, W.; Wang, S.; Toh, M.; Ribeiro, R. M.; Neto, A. C.; Matsuda, K., Photocarrier Relaxation Pathway in Two-Dimensional Semiconducting Transition Metal Dichalcogenides. *Nat. Commun.* **2014**, *5*, 4543.
43. Carvalho, A.; Ribeiro, R. M.; Neto, A. H. C., Band Nesting and the Optical Response of Two-Dimensional Semiconducting Transition Metal Dichalcogenides. *Phys. Rev.B* **2013**, *88*, 115205.
44. Frindt, R. F., Single Crystals of MoS₂ Several Molecular Layers Thick. *J. Appl. Phys.* **1966**, *37*, 1928-1929.
45. Zhang, Y.; Sun, Y.; Zhong, B., Synthesis of Higher Alcohols from Syngas over Ultrafine Mo—Co—K Catalysts. *Catal. Lett.* **2001**, *76*, 249-253.
46. Benoist, L.; Gonbeau, D.; Pfister-Guillouzo, G.; Schmidt, E.; Meunier, G.; Levasseur, A., XPS Analysis of Lithium Intercalation in Thin Films of Molybdenum Oxysulphides. *Surf. Interface Anal.* **1994**, *22*, 206-210.
47. Bae, S.; Kim, H.; Lee, Y.; Xu, X.; Park, J.-S.; Zheng, Y.; Balakrishnan, J.; Lei, T.; Kim, H. R.; Song, Y. I., Roll-To-Roll Production of 30-Inch Graphene Films for Transparent Electrodes. *Nat. Nanotechnol.* **2010**, *5*, 574-578.
48. Kim, Y. E.; Park, H.; Kim, J. J., Enhanced Quantum Efficiency in Polymer Electroluminescence Devices by Inserting a Tunneling Barrier Formed by Langmuir–Blodgett Films. *Appl. Phys. Lett.* **1996**, *69*, 599-601.

49. Zhan, D.; Sun, L.; Ni, Z. H.; Liu, L.; Fan, X. F.; Wang, Y.; Yu, T.; Lam, Y. M.; Huang, W.; Shen, Z. X., FeCl₃-Based Few-Layer Graphene Intercalation Compounds: Single Linear Dispersion Electronic Band Structure and Strong Charge Transfer Doping. *Adv. Funct. Mater.* **2010**, 20, 3504-3509.
50. Zhang, W.; Lin, C.-T.; Liu, K.-K.; Tite, T.; Su, C.-Y.; Chang, C.-H.; Lee, Y.-H.; Chu, C.-W.; Wei, K.-H.; Kuo, J.-L., Opening an Electrical Band Gap of Bilayer Graphene with Molecular Doping. *ACS Nano* **2011**, 5, 7517-7524.
51. Ryu, S.; Liu, L.; Berciaud, S.; Yu, Y.-J.; Liu, H.; Kim, P.; Flynn, G. W.; Brus, L. E., Atmospheric Oxygen Binding and Hole Doping in Deformed Graphene on a SiO₂ Substrate. *Nano Lett.* **2010**, 10, 4944-4951.
52. Pu, J.; Yomogida, Y.; Liu, K.-K.; Li, L.-J.; Iwasa, Y.; Takenobu, T., Highly Flexible MoS₂ Thin-Film Transistors with Ion Gel Dielectrics. *Nano Lett.* **2012**, 12, 4013-4017.
53. Das, S.; Chen, H.-Y.; Penumatcha, A. V.; Appenzeller, J., High Performance Multilayer MoS₂ Transistors with Scandium Contacts. *Nano Lett.* **2012**, 13, 100-105.
54. Fu, D.; Zhou, J.; Tongay, S.; Liu, K.; Fan, W.; Liu, T.-J. K.; Wu, J., Mechanically Modulated Tunneling Resistance in Monolayer MoS₂. *Appl. Phys. Lett.* **2013**, 103, 183105.
55. Yu, Y.-J.; Zhao, Y.; Ryu, S.; Brus, L. E.; Kim, K. S.; Kim, P., Tuning the Graphene Work Function by Electric Field Effect. *Nano Lett.* **2009**, 9, 3430-3434.

Supporting Information

Enhanced Photovoltaic Performances of Graphene/Si Solar Cells by Insertion of an MoS₂ Thin Film

Yuka Tsuboi[†], Feijiu Wang[†], Daichi Kozawa[†], Kazuma Funahashi[‡],
Shinichiro Mouri[†], Yuhei Miyauchi[†], Taishi Takenobu[‡] and Kazunari Matsuda^{†*}

[†]*Institute of Advanced Energy, Kyoto University, Gokasho, Uji, Kyoto 611-0011, Japan*

[‡]*Department of Advanced Science and Engineering, Waseda University, Shinjuku-ku, Tokyo 169-
8555, Japan*

[§]*JST, ERATO, Itami Molecular Nanocarbon Project, Nagoya University, Chikusa, Nagoya 464-
8602, Japan*

*Email: matsuda@iae.kyoto-u.ac.jp

S1. MoS₂ film fabrication

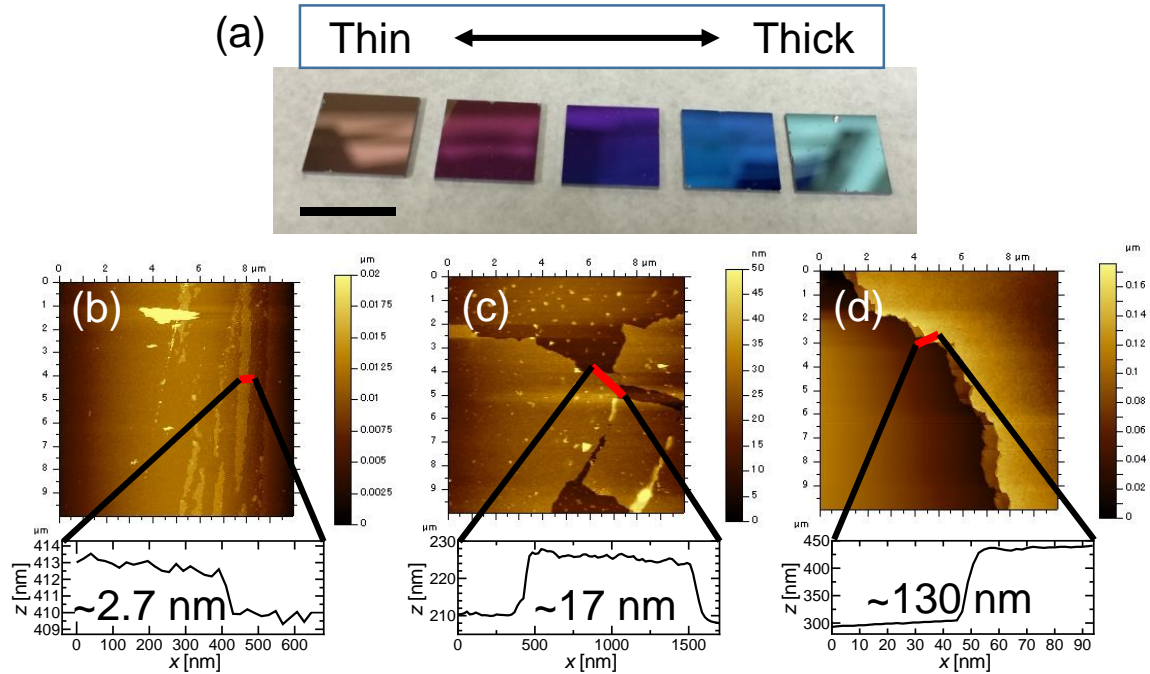


Figure S1. (a) Optical image of as-grown MoS₂ films with various layer thicknesses on SiO₂/Si substrates, as fabricated by the CVD method. The scale bar is 1 cm. The thickness of the MoS₂ films was controlled *via* the MoO₃ deposition time. The leftmost image is an SiO₂/Si substrate. (b)–(d) AFM images of an MoS₂ film. The height profiles are measured at the step edge between the MoS₂ film and the SiO₂/Si substrate. The thickness of the MoS₂ films was varied from 2.7 to 130 nm. For solar cells in Figure 3, we used films with ~17-nm thickness, as shown in (c).

S2. Process-flow of MoS₂ film transfer

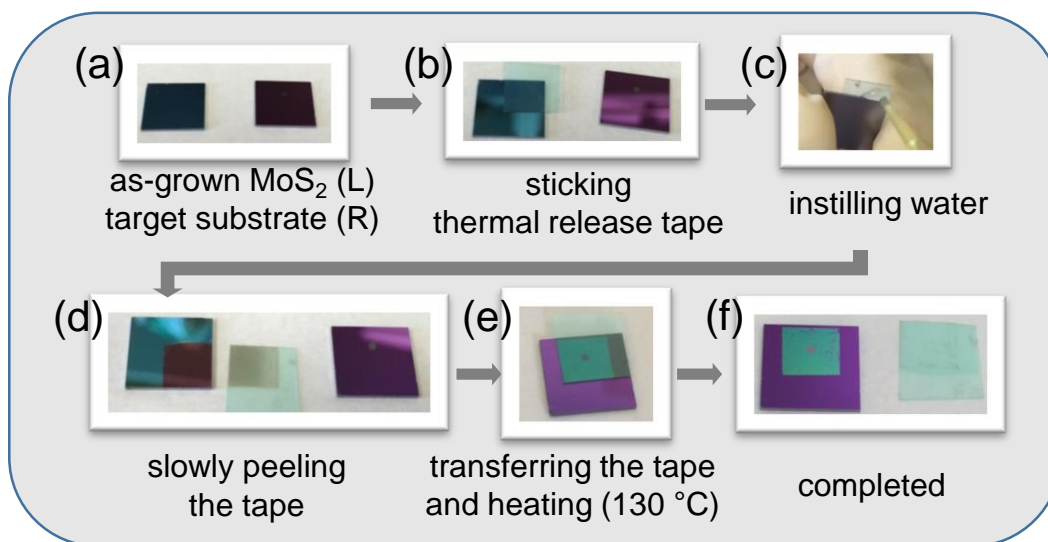


Figure S2. (a)–(f) The process-flow of as-grown MoS₂ film transfer. This method was conducted using thermal release tape (REVALPHA; No. 3195MS, Nitto Denko). The sticking MoS₂ film with the thermal release tape (left in (b)) was easily released by a drop of water, as shown in (c). After the tape with MoS₂ was transferred to the target substrate, the tape was removed by heating the substrate on a hotplate.

S3. Characterization of stacked graphene/MoS₂ film

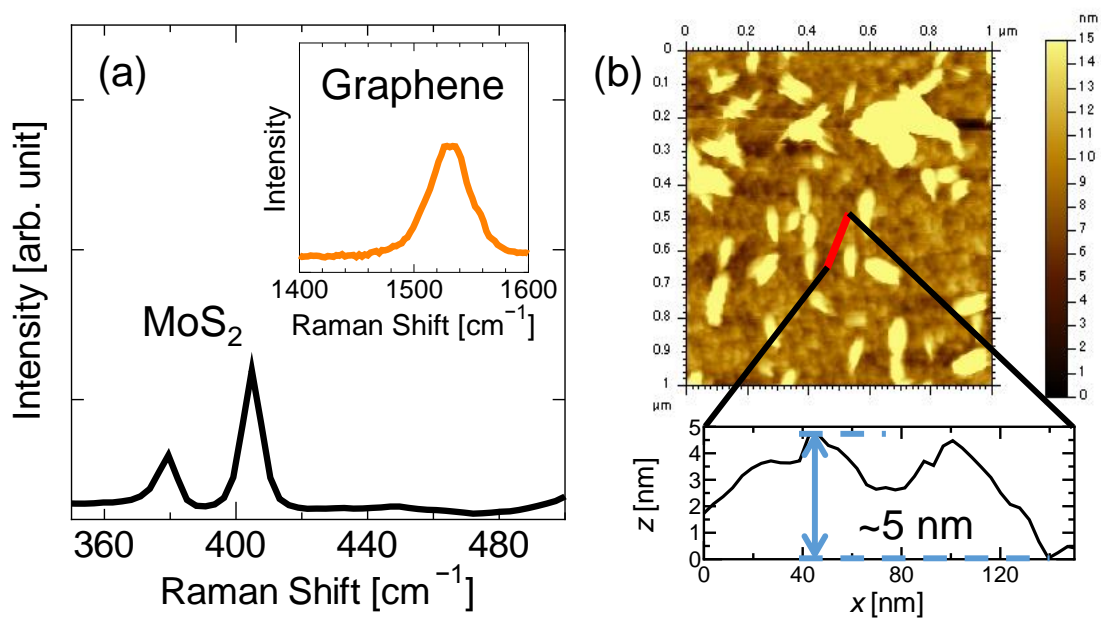


Figure S3. (a) Raman spectrum of the vertical stacking of graphene/MoS₂. (b) AFM image of a stacked graphene/MoS₂ film and its height profile along the red line in the image. The surface roughness of the graphene/MoS₂ film decreases in comparison with that of the MoS₂ film (Figure 2(a)).

S4. Photovoltaic parameters of graphene/MoS₂/*n*-Si solar cells

Table S4. Photovoltaic parameters of graphene/MoS₂/*n*-Si solar cells with monolayer-graphene (MLG), bilayer-graphene (BLG) and trilayer-graphene (TLG), as evaluated from experimentally obtained J - V curves. The open-circuit voltage V_{OC} , short-circuit current density J_{SC} , fill factor FF, photovoltaic efficiency η , and series resistance R_S are shown. Here, the R_S values were estimated from the slopes of the J - V curves.^{S1}

Cell Type	V_{OC} [V]	J_{SC} [mA/cm ²]	FF	η [%]	R_S [W·cm ²]
MLG/MoS ₂ / <i>n</i> -Si	0.41	13.1	0.25	1.35	30
BLG/MoS ₂ / <i>n</i> -Si	0.51	21.4	0.55	5.98	11
TLG/MoS ₂ / <i>n</i> -Si	0.54	28.2	0.53	8.02	8.8

S5. The incident photon-to-current conversion efficiency (IPCE) spectrum of graphene/MoS₂/*n*-Si solar cells

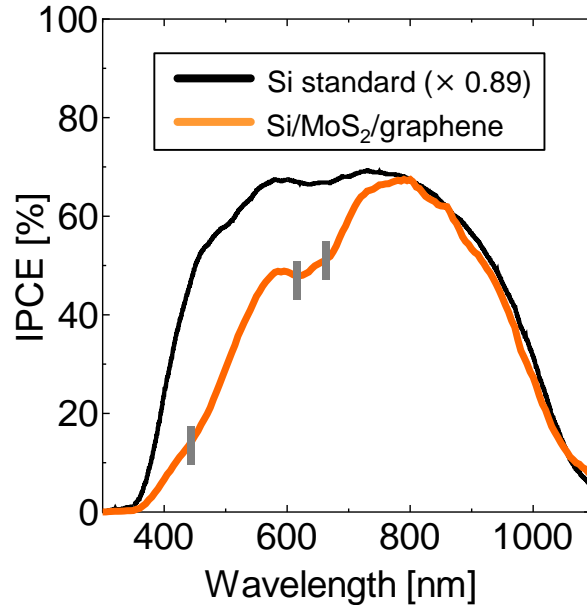


Figure S5. IPCE spectra of a trilayer-graphene/MoS₂/*n*-Si solar cell and a standard Si solar cell. The spectrum of the standard Si solar cell is normalized by the values at 800 nm. The dip structures were observed in the IPCE spectrum of graphene/MoS₂/*n*-Si in the shorter-wavelength region (400–700 nm). The positions of these dip structures are consistent with the absorption peaks of the MoS₂ film shown in Figure 2(b), which suggests that the generated carriers in the *n*-Si layer are the primary contributors to the photovoltaic current in the cell, whereas the MoS₂ functions as a shading layer at the point of light absorption.

S6. Carrier transport properties of an MoS₂ film, as measured by an electric double-layer transistor

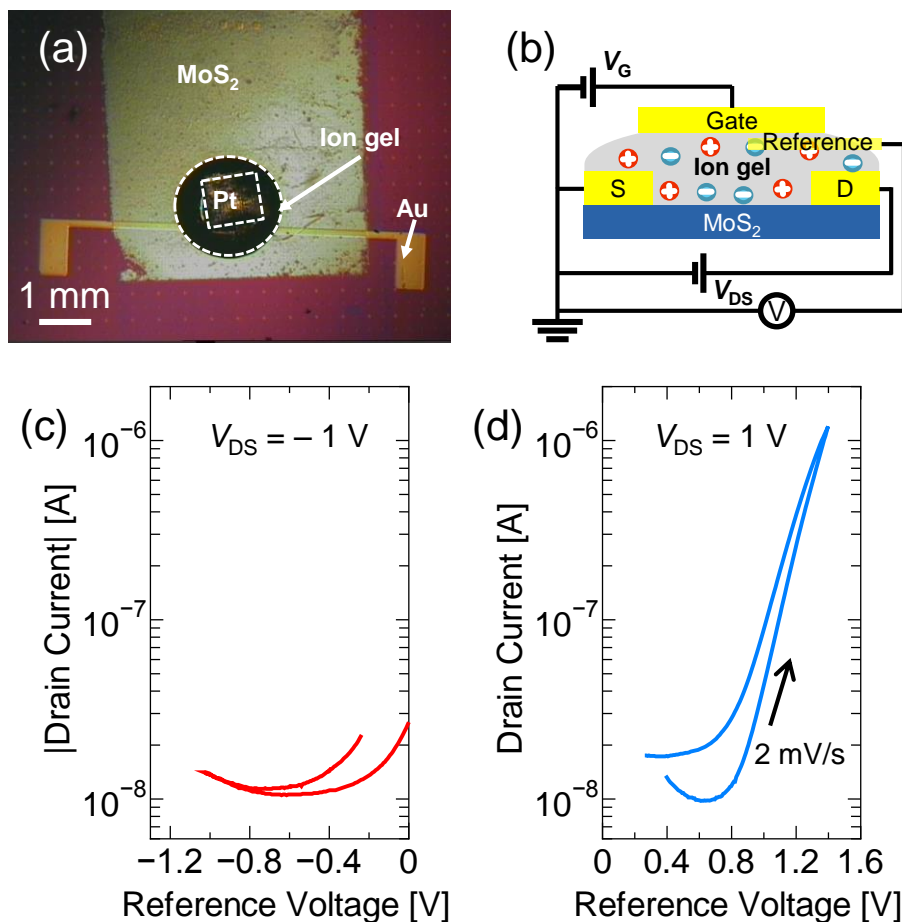


Figure S6. (a) Optical image of CVD-grown MoS₂ electric double-layer transistor and (b) A schematic illustration of the transistor, in which an ionic gel ([EMIM][TFSI] with PS-PMMA-PS) as a gate electrolyte, Pt as a top-gate electrode, and Ni/Au source and drain electrodes were used.^{S2} (c)(d) Transfer characteristics measured by changing the voltage of the Pt top-gate electrodes. Current resulting from electron transfer was confirmed (blue line), whereas current resulting from hole transfer was not (red line).

Reference

- S1. Miao, X.; Tongay, S.; Petterson, M. K.; Berke, K.; Rinzler, A. G.; Appleton, B. R.; Hebard, A. F., High Efficiency Graphene Solar Cells by Chemical Doping. *Nano Lett.* **2012**, 12, 2745-2750.
- S2. Pu, J.; Yomogida, Y.; Liu, K.-K.; Li, L.-J.; Iwasa, Y.; Takenobu, T., Highly Flexible MoS₂ Thin-Film Transistors with Ion Gel Dielectrics. *Nano Lett.* **2012**, 12, 4013-4017.